University of Zagreb

Doctoral Thesis

Measurement of the cross section for associated production of a W boson and two b quarks with the CMS detector at the Large Hadron Collider

Author:

Jelena Luetic

Supervisor:

Dr. Vuko Brigljevic

A thesis submitted in fulfilment of the requirements for the degree of Doctor of Philosophy

in the

Research Group Name

Faculty of Science

February 2015

"Thanks to my solid academic training, today I can write hundreds of words on virtually any topic without possessing a shred of information, which is how I got a good job in journalism."

Dave Barry

UNIVERSITY OF ZAGREB

Abstract

Faculty Name
Faculty of Science

Doctor of Philosophy

Measurement of the cross section for associated production of a W boson and two b quarks with the CMS detector at the Large Hadron Collider

by Jelena Luetic

The Thesis Abstract is written here (and usually kept to just this page). The page is kept centered vertically so can expand into the blank space above the title too...

Acknowledgements

The acknowledgments and the people to thank go here, don't forget to include your project advisor…

Contents

List of Figures

List of Tables

For my Gogi.

Chapter 1

Introduction

Chapter 2

Theoretical overview

Standard model of elementary particles is a theory emerged in 1960s and 1970s describing all of the known elementary particles and interactions except gravity. The final formulation of Standard model incorporates several theories: quantum electrodynamics, Glashow-Weinberg-Salam theory of electroweak processes and quantum chromodynamics, all of them describing the relations between quarks and fermions. First steps towards formulation of Standard model occurred in 1960. when Sheldon Glashow unified electromagnetic and weak interactions. In 1967. Steven Weinberg and Abdul Salam are using Higgs mechanism in the electroweak theory explaining the origin of mass for elementary particles. After discovery of neutral currents which arise from the exchange of the neutal Z boson, electroweak theory becomes generally accepted. W and Z bosons were discovered in 1981 at CERN, and their masses were in agreement with the Standard model prediction. Theory describing strong interactions got itćs final form in 1974. when it was shown that hadrons are consisting of quarks. There are evidences which show the Standard model is not a final theory of elementary particles, but so far it's predictions were confirmed every time through numerous experimental tests. Standard model has one additional nice property, all fundamental interactions arise from one general principle, the requirement of local gauge invariance.

In this chapter a brief overview of the standard model particles and interactions will be shown with the emphasis on the W boson and b quarks which are the most relevant for this thesis. Cross section determination at hadron colliders will be shown. In the last part of the chapter historical account of the development of W+b-jets theoretical calculations is described together with the existing experimental results.

2.1 Standard model overview

Elementary particle physics is described within a framework of standard model. We usually imagine particles as point like objects and some forces between them. Particles, or matter, are fermions, leptons of quarks of spin $s = 1/2$. There are three charged leptons, electron, muon and tau which properties are the same except for their mass. Each of the leptons has a corresponding neutrally charged neutrino which has a very small mass. There are six different types of quarks with charge either $Q = 2/3$ of $Q = -1/3$. They also carry one additional quantum number which is color charge. All objects observed in nature are colorless giving raise to the concept of quark confinement. Colorless composite objects are classifies into two categories. Bayons are fermions which are made out of three quarks, for example proton or neutron. The other category are mesons which are made of two quarks like pions. Matter is divided into three categories which are identical except for the masses of the particles.

From the point of view of the quantum field theory, standard model is based on a gauge symmetry $SU(3)_C \times SU(2)_L \times U(1)_Y$. Strong interaction is described by $SU(3)_C$, while electroweak sector is described by $SU(2)_L \times U(1)_Y$. All interactions within Standard Model are mediated by an elementary particle which is a spin 1 boson. In the case of electromagnetic interaction, mediator is massless photon thus the range of electromagnetic interaction is infinite. For weak force mediators are three massive bosons $W^{\pm}$ and Z and it's range is very small (10^{-16}). These four bosons are the gauge bosons of $SU(2)_L \times U(1)_Y$ group. The interaction between electroweak bosons is allowed in the Standard Model in a way that charge conservation principle remains valid. Strong force is mediated by the exchange of 8 massless gluons which are gauge bosons for $SU(3)_C$. Although gluons are massless, the range of the strong force is not infinite. Because of the effect of confinement, the range of the strong force is approximately the size of the lightest hadrons $(10^{-}13cm)$.

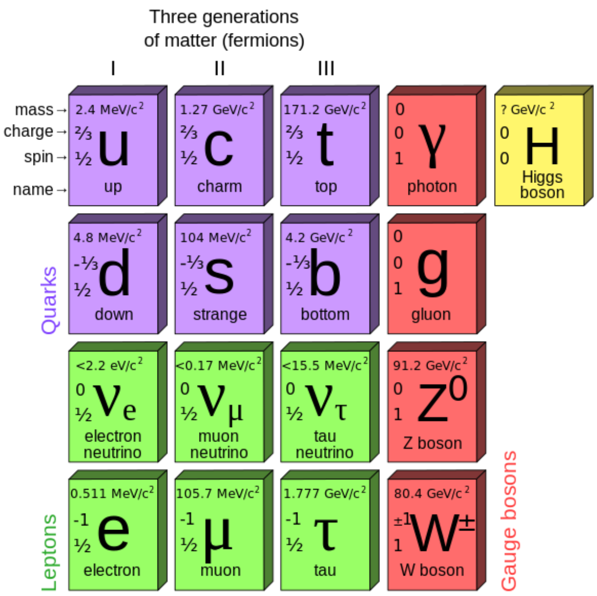

FIGURE 2.1: List of Standard model elementary particles.

Scalar sector of the standard model has been experimentally confirmed only recently [1, 2]. The fact that weak gauge bosons are massive indicates that $SU(2)_L \times U(1)_Y$ is not a good symmetry of the vacuum. In contrast with photon being massless, $U(1)_em$ is a good symmetry of the vacuum which means that $SU(2)_L \times U(1)_Y$ electroweak symmetry is somehow spontaneously broken to $U(1)_em$ of electromagnetism. Spontaneous symmetry breaking is implemented through Higgs mechanism which gives masses to $W\pm$ and Z boson, fermions and leaves photon massless. The details of the mechanism can be found elsewhere [3] but the main point is that the mechanism also predicts a new scalar and electrically neutral particle which is called Higgs boson. The search for Higgs boson lasted few decades before finally in 2012, a new particle was discovered with mass of 125 GeV. In subsequent years, properties of this new particle have been measured and at this point, all measurements agree with Standard Model predictions for Higgs boson.

2.1.1 Bottom quarks

Bottom quark was first predicted by Makoto Kobayashi and Toshihide Maskawa in 1974 when extending Cabbibo weak mixing angle to take into account CP violation observed in neutral K mesons. [4] The name "bottom" was introduced in 1975 by Haim Harari. The bottom quark was discovered in 1977 by the Fermilab E288 experiment team led by Leon M. Lederman through the observation of Υ resonance. [5] Kobayashi and Maskawa won the 2008 Nobel Prize in Physics for their explanation of CP-violation.

At the the LHC, the main production mechanism for b quarks is through strong interaction ($g \to bb$) and top quark decay ($t \to Wb$). Every b quark, after production, goes through the process of hadronisation, forming one of the color neutral B mesons. B meson decays electromagnetically if produced in excited state to the ground state. Lowest state B mesons decay weakly, resulting in relatively long lifetime of 1.5 ps. According to CKM matrix 2.1, b quark can decay either to c quark ($\approx 95\%$ of the cases) or u quark ($\approx 95\%$ of the cases). Long lifetime of b quark makes it possible to traverse a substantial distance inside the detector. This fact is used in the creation of various b-tagging algorithms which are taking into account tracks originating from displaced verices, discussed in Section 4.

$$\begin{pmatrix} V_{ud} & V_{us} & V_{ub} \\ V_{cd} & V_{cs} & V_{cb} \\ V_{td} & V_{ts} & V_{tb} \end{pmatrix} = \begin{pmatrix} 0.974 & 0.225 & 0.003 \\ 0.225 & 0.973 & 0.041 \\ 0.009 & 0.040 & 0.999 \end{pmatrix} \tag{2.1}$$

2.1.2 Discovery and role of W boson

W boson is one of the massive mediators of weak interaction with a mass of $m_W = 80.1$ GeV. The theory of the weak interactions got it's final form in 1968 when Sheldon Glashow, Steven Weinberg, and Abdus Salam unified a theory of electromagnetism and weak interactions. The discovery of W and Z bosons at UA1 and UA2 experiments was one of the major successes of the CERN experimental facility. Super Proton Synchrotron was the first accelerator powerful enough to produce W and Z bosons. Both collaborations reported their findings in 1983 [6, 7]. W boson at the LHC is primarily produced through quark-antiquark annihilation. In majority of the cases, W boson decays to quark-antiquark pair (66%). Other decay channels include creation a lepton and it's corresponding neutrino($\approx$ 10% per lepton generation). This decay channel was the most important for W boson discovery and it's still essential for W boson detection at hadron colliders despite the large hadronic backgrounds.

Study of W+jets production at hadron colliders started in 1980s motivated by the top quark searches. Additional jets either come from radiation of additional quarks or gluons. However, because they carry color charge, quarks and gluons undergo the process of parton shower and hadronization forming jets in the detector. Parton shower is the process in which a high energy colored particle emits a low energy colored particle while hadronization is the process in which colored particle combine to form color neutral particles. Parton shower and hadronization cannot be computed analytically, but have to be modeled using Monte Carlo simulations. As a result of these processes, in the final state there can be a number of jets that doesn't correspond to the number of incoming partons. This becomes relevant when trying to form an inclusive W+jets sample from exclusive (W + 1 jet, W + 2 jets...) samples and some process of matching has to be performed in order to avoid double counting. Matching procedure is described in detail in [8].

Many theoretical issues arise when trying to compute cross sections for W+jets processes. Divergences while calculating amplitudes come from emission of soft particles or collinear jets. These problems are solved by introducing a cut-off called factorization scale. Other divergences come from integrating higher-order loops. Usually this type of divergence is than included into renormalized coupling constant. This procedure, however introduces a certain scale dependence into the result which will be discussed further in Section 2.2.1.

2.2 W + b jets at hadron colliders

First theoretical computations of W boson in association with b jets were published in 1993 [9], however only recently enough luminosity has been collected at hadron colliders to be able to make cross section measurements. This process was first interesting as a background to top quark searches and measurements where top quark decays to W boson and a b quark. In past few years, with the Higgs boson discovery, an important open question is whether the new particle also couples to fermions, and in particular to bottom quarks. Determination of this coupling requires direct measurement of the corresponding Higgs boson decay, as recently reported by the CMS experiment in the study of Higgs decays to bottom quarks [10, 11]. Standard model Higgs boson branching ratio for decays into a bottom quark-antiquark pair (bb) is $\approx 58\%$. Study of this decay channel is therefore essential in determining the nature of the newly discovered boson. The measurement of the H $\rightarrow$ bb decay will be the first direct test of whether the observed boson interacts as expected with the quark sector, as the coupling to the top quark has only been tested through loop effects. However, the large backgrounds for this measurement make it essential that all the contributing processes including W+b jets are well understood. There are also Beyond Standard Model searches where contributions from this process is substantial including some Supersymmetry searches with lepton, b jets and missing energy in the final state.

Soft and collinear divergences are naturally avoided in processes with b jets because of relatively high mass of b quark which means that the scale of the process doesn't go below $2m_b$.

2.2.1 Cross sections at hadron colliders

Determining cross sections for processes at hadron collides is not an easy task. With proton being a composite object consisting of partons, it is necessary to include it's internal structure as well as the diagrams for hard scattering of interest. This means soft and hard processes are occurring in the same event. Quarks and gluons within proton interact through strong force and are described using quantum chromodynamics. Two processes make it possible to perform calculations within the QCD, asymptotic freedom and factorization theorem. Since strong force coupling constant α_s depends on the scale, for high momentum transfers ($Q >> \Lambda_{QCD} \approx 200\text{MeV}$) it becomes sufficiently small to make perturbative expansion in α_s possible. This feature is called asymptotic freedom and it is used to determine the hard process cross section. Figure 2.2 shows the results of the α_s measurements which is in complete agreement with the QCD predictions of asymptotic freedom.

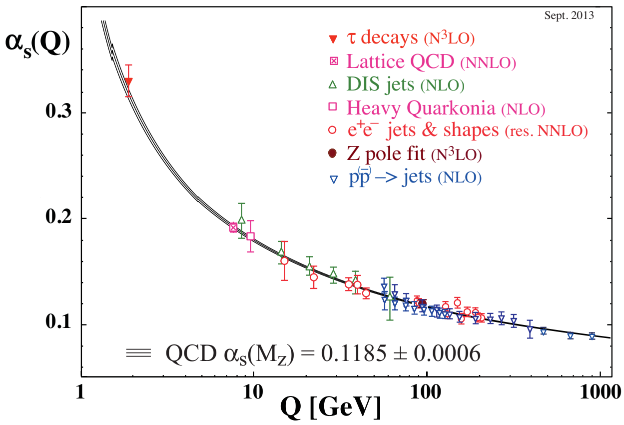

FIGURE 2.2: Summary of measurement of strong coupling constant α_s [12]

Perturbative QCD cannot be used if the momentum transfer values are small and the coupling constant becomes large. This phenomenon is called *confinement* and it requires different treatment for the quarks inside the proton. Internal structure of a proton is described using parton distribution functions which are determined through deep inelastic scattering experiments. Parton distribution functions for each of the partons inside a proton is shown in Figure 2.3 made with one specific PDF function(MSTW). Using DGLAP equations, it is possible to evolve the PDFs for any momentum transfer value which is described in detail in [13]

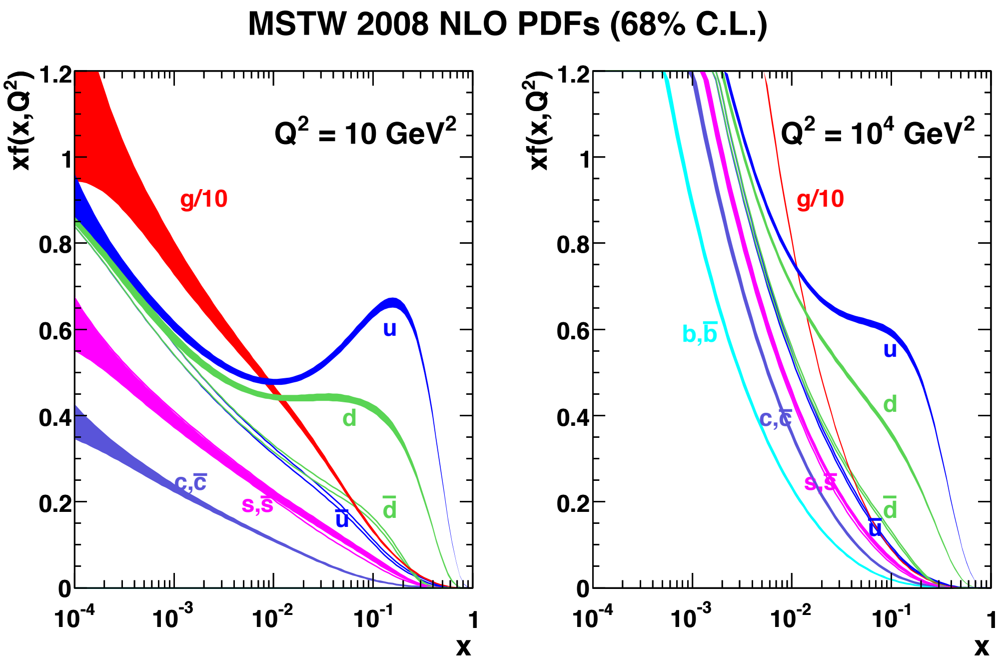

FIGURE 2.3: Parton distribution functions calculated by the MSTW group for $Q = 10\text{GeV}$ and $Q = 10^4\text{GeV}$ [14]

While performing perturbative QCD calculations, it is important to impose conditions to the final state in order to avoid soft and collinear divergences. Collinear divergences originate from configurations with a small opening angle between jets. Soft divergences appear when quark or gluon is irradiated at low momentum. Factorization scale is introduced as a cut-off for diagram calculation below which perturbative QCD calculation is not performed which means that hard scattering between partons is independent from the parton internal structure. The main point of the factorization theorem is that because of energy dependence of strong coupling constant, hard and soft part of the process are happening at different time scales ans soft part is factorized inside a parton distribution function. Drawing of a proton proton collision is shown in figure 2.4. If we want to calculate the cross section for some process where there are two protons in the initial state and some interesting final state which we call X, according to [13], necessary steps are:

1. Identify the leading order partonic processes that contribute to X

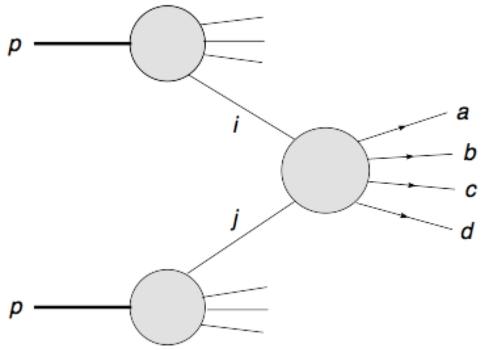

FIGURE 2.4: Drawing of a proton-proton collision.

2. Calculate the corresponding hard scattering cross section
3. Determine the appropriate PDFs for initial state partons
4. Make a specific choices for factorization(μ_F) and renormalization(μ_R) scales
5. Perform integration over the fraction of momentum available for a given parton(x)

The cross section at hadron collides is thus a convolution of the hard scattering perturbative cross section and two incoming parton distribution functions.

$$\sigma_{AB} = \sum_{n=1}^{\infty} \alpha_s^n(\mu_R^2) \sum_{i,j} \int dx_1 dx_2 f_{i/A}(x_1, \mu_F^2) f_{j/B}(x_2, \mu_F^2) \sigma^{(n)}_{ij\to X}(x_1 x_2 s, \mu_R^2, \mu_F^2) \tag{2.2}$$

Equation 2.2 shows cross section perturbation series in α_s, n denotes the order of the series where $n = 1$ is leading order, $n = 2$ is next to leading order, etc. Hard process cross section between two partons $\sigma^{(n)}_{ij\to X}$ is computed in the framework of perturbative QCD and depends on s which is squared center of mass energy. Two parton distribution functions are denoted with $f_{i/A}$ and $f_{j/B}$ and correspond to the probability density that parton $i(j)$ with proton momentum fraction $x_1(x_2)$ will be found inside a proton. Sum over all combinations of partons has to be computed. Integral over available phase space for proton fraction momentum dx is usually carried out by simulations.
Here μ_F represents *factorization scale* and μ_R is *renormalization scale* for running coupling

constant. They are arbitrary cut-offs used to remove nonperturbative effects and be able to make perturbative calculations. If cross section is computed in full series, μ_F and μ_R should cancel out, and scale dependence should disappear. However, since fewer orders are used and some residual scale dependence is still present. This dependency can be used to estimate the contribution of the missing orders in the series.

Usually factorization and renormalization scales are chosen to be identical and close to the scale of the process in question.

NAPISATI PRIRODNE IZBORE SKALE!!!

Figure 2.5 shows some interesting Standard model cross sections in proton-proton and proton-antiproton collisions as a function of a center of mass energy. All cross sections have been computed to the NLO order using the above described procedure.

2.2.2 Contributions to Wbb cross section

From theoretical point of view, calculations of W+b jets processes can be divided into two categories: only light quarks in the initial state shown in figure 2.6 (four flavour scheme - 4FS) and b quark in the initial state, usually called five flavor scheme (5FS) shown in Figure 2.9. Additional contribution to Wbb production at hadron colliders comes from double parton interactions where a W boson and a pair of b quarks is produced in different hard process inside the same collision as shown in Figure 2.10. This contribution will be discussed in Section 2.2.2.1.

The rationale behind using 4FS or 5FS is discussed in detail in [15]. Four flavor scheme approach assumes that bottom quarks are heavy and can only be created as pairs in collisions with high momentum transfer or as a decay product of t quark. Heavy quarks are not included in the initial state and their parton distribution function is set to zero which means an effective theory is created where heavy quarks do not enter the computation of running coupling and the evolution of PDFs. In this approach, it is assumed that scale is of the same order as the other hard scales in the process. If it happens

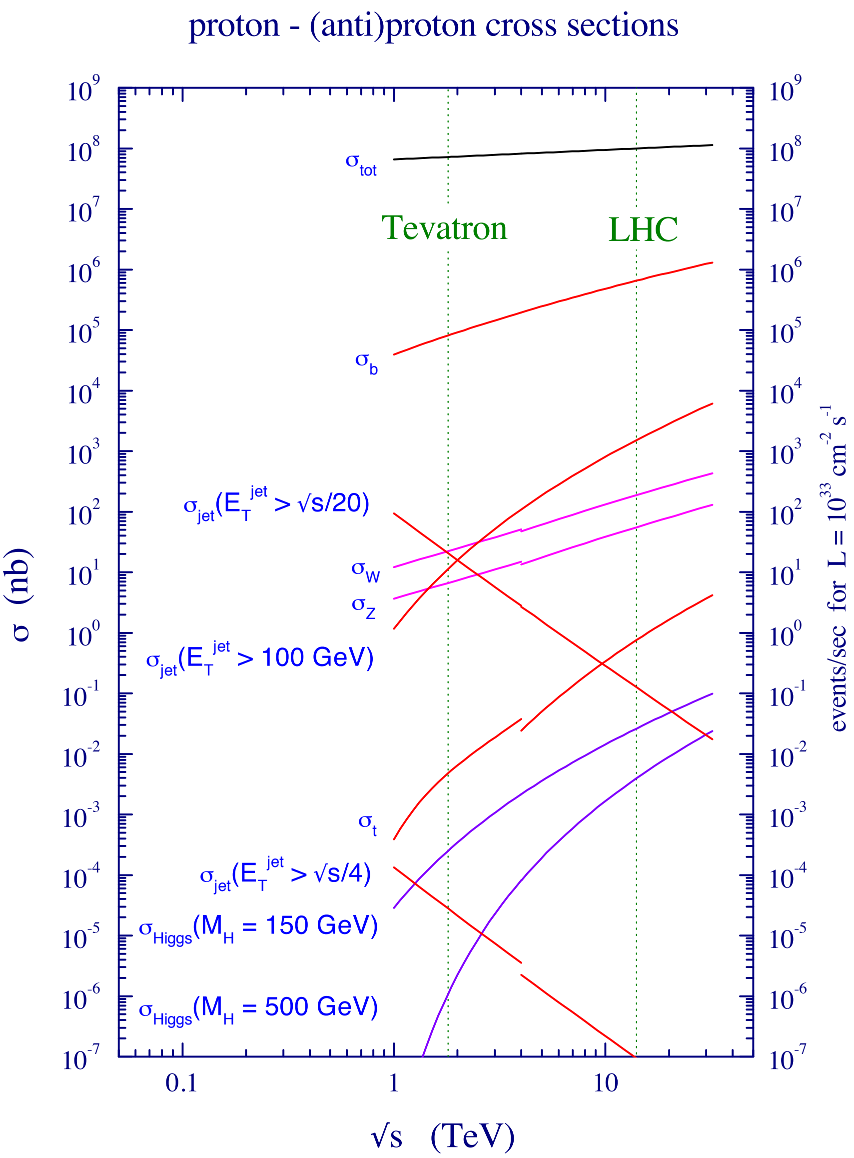

FIGURE 2.5: Standard model cross sections as a function of center of mass energy.[13]

that the scale of the process if much higher than the mass of the b quark, for example in the production of massive bosons, large logarithms of the type $log(Q^2/m_b^2)$ appear and can spoil the convergence of a fixed order perturbative expansion and it introduces large scale dependence into the final result. In five flavor schemes calculations include b quark in the initial state which means some new and simpler processes become available. These calculation allow ressumation of possibly large logarithms of type $log(Q^2/m_b^2)$ into the b quark parton distributions function possibly transforming some higher order calculations into much simpler leading order calculations. Their results show that at the LHC 4-flavor calculations are well behaved and two schemes are in good agreement. The typical size of the possibly problematic logarithms in four flavor scheme in hadron colliders is not large enough to spoil convergence. On the other hand, five flavor scheme is less dependant on the scale of the process and show smaller uncertainties which is in general very good for predictions of inclusive observables.

First leading order calculations for associated production of a W boson and heavy quarks at hadron colliders were presented in 1993. Feynmann diagram for leading order W + 2 b jets production is shown in Figure 2.6. Exact leading order matrix element has been computed and higher order corrections were estimated using Monte Carlo. Their results are summarized in the Figure 2.7 where the differential cross section for W+2 b jets as a function of a leading b jet p_T is shown. Two scale choices have been studied, first one with $\mu_0 = M_{bb}$ which is the invariant mass of the dijet system and is represented with solid line. Second choice is $\mu_0 = m_W + p_T^W$ and is represented with the dotted line. Looking at the normalizations of two diagrams, the difference is clearly visible which indicates a strong total cross section scale dependence. However, the shape of the differential cross section shows the same behavior in both cases which means that the scale only affects total cross section.

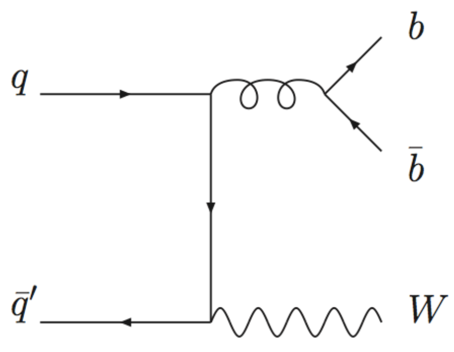

FIGURE 2.6: Leading order Wbb Feynmann diagram

Later development of theoretical calculations was strongly motivated by reducing the scale dependence of the result and it included adding additional partons to the final

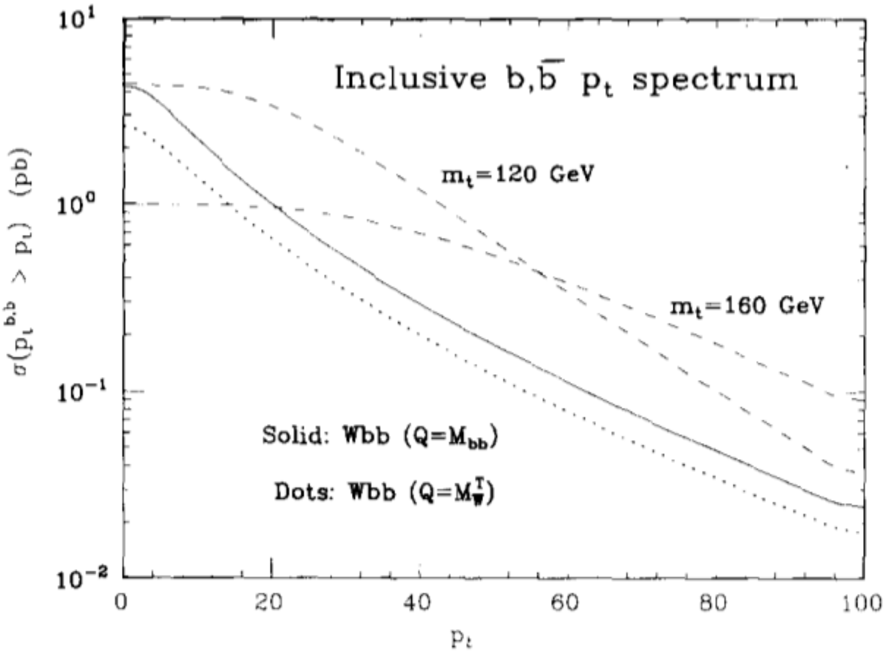

FIGURE 2.7: Scale dependence of Wbb cross section

state. This was a first step towards the full NLO calculation. The only thing missing was taking into account the loop effects. This approach made it possible to access some previously inaccessible kinematics, however at the expense of introducing additional scale dependence. The list of new final states is simple and it includes $Wbbq$, $Wbbq\bar{q}$, $Wbb\bar{q}q'\bar{q}'$... For the measurements at the LHC in particular, calculations for new initial states qg and gg were of great importance. First results for W+2 jets were published in [16]. Additional calculations were shown in [17] for up to six additional jets in the final state. Although these processes are suppressed by an additional α_s factor, the gluon PDF inside a proton is much larger than anti-quark, so this production mechanism is significant at the LHC energies.

First full NLO calculations were published in 2006[18]. Events with b jet pair in the final state were selected, with of the dijet system p_T >15 GeV and a pseudorapidity less than 2. The results were shown for two categories, inclusive and exclusive, depending on the treatment of extra jets. In the inclusive case events with additional jets were included, while in the exclusive case exactly two jets were required. Figure 2.8 shows the overall scale dependence of LO, NLO inclusive and NLO exclusive total cross-ections, when both renormalization scale and factorization scale are varied independently between $\mu 0/2$ and $4\mu 0$ (with $\mu 0 = m_b + M_W/2$), including full bottom-quark mass effects. NLO cross sections have a reduced scale dependence over most of the range of scales shown, and the exclusive NLO cross-section is more stable than the inclusive one especially at low scales. This is consistent with the fact that the inclusive NLO cross-section integrates over the entire phase space of the $qg(\bar{q}g) \rightarrow \bar{b}bW + q(\bar{q})$ channels that are evaluated with NLO α_s and NLO PDF, but are actually tree-level processes and retain therefore a strong scale dependence. The effect of the b quark mass has been shown to affect the total NLO cross section on the order of $\approx 8\%$. This is expected to be small when considering well separated jets.

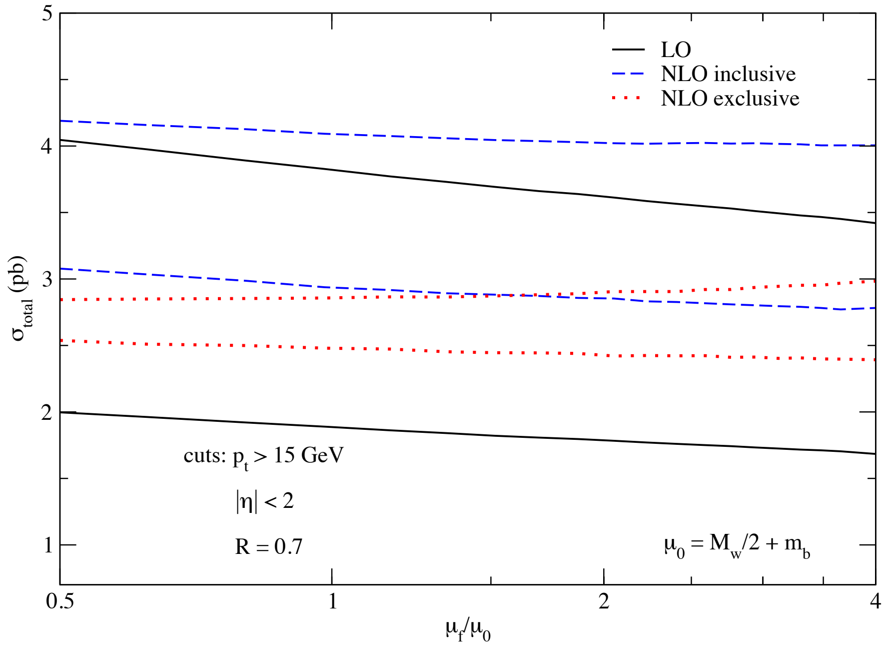

FIGURE 2.8: Wbb NLO scale dependence[18]

New results published in 2007 explored in particular NLO corrections for events with W boson and two jets where at least one is b-tagged. It was shown that for LHC the correction factor is ≈ 1.9. This paper was interesting in particular for it's study of soft and collinear topologies, where two b quarks merge into one. Additionally, b quark in the initial state was considered giving rise to the processes like $bq \to Wbq'$ shown in figure 2.9. Parton distribution function for b quark needed to be determined perturbatively using DGLAP equations. Other approach is to consider a gluon in the initial state which then splits to $b\bar{b}$.

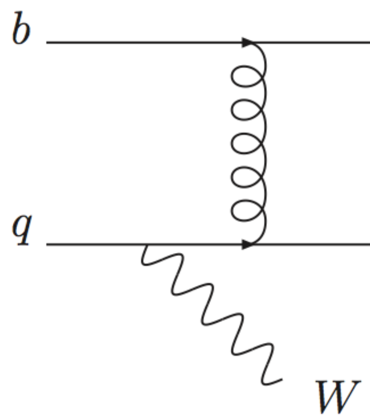

FIGURE 2.9: Wbb production within 5 flavor scheme

2.2.2.1 Double parton scattering

Multiple parton interactions happen due to composite nature of the proton. Usually inside a proton, only one parton has significant fraction of proton momentum x to produce a hard scattering. However, sometimes can happen that two such partons exist which results in two hard scatterings in the same collisions. This phenomenon is called Double Parton Scattering (DPS) and is shown in Figure 2.10. In the framework of this thesis, this means that two partons are responsible for creation of a W boson and other two for creation of pair of b jets.

Double parton scattering cannot be modeled in the framework of preturbative QCD, but it is approximated using simulations. The phenomenology of DPS starts from the assumption that factorization between two hard processes is possible, as well as factorization between hard processes and proton kinematics. Cross sections for hard scatterings

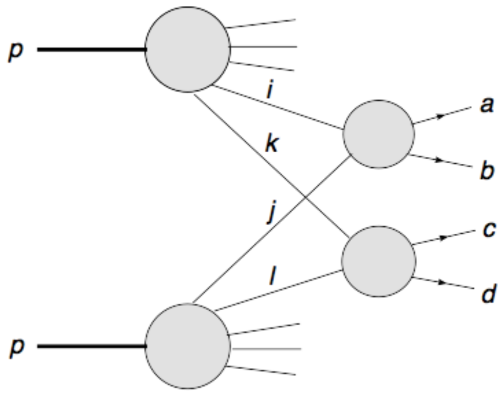

FIGURE 2.10: Double parton scattering

are computed separately of each pair of partons. However, instead of using regular parton distribution functions, a new set of distribution functions has been defined which are called Double Parton Distribution Functions (dPDFs). Factorized cross section for two hard processes A and B to happen in proton-proton scattering can be written as:

$$\begin{aligned}\sigma^{DPS}_{(A,B)} \sim \sum_{i,j,k,l} \int dx_1 dx_2 dx'_1 dx'_2 d^2b \Gamma_{ij}(x_1, x_2, b; Q_1, Q_2) \sigma^A_{ik}(x_1, x'_1) \\ \sigma^B_{jl}(x_2, x'_2) \Gamma_{kl}(x'_1, x'_2, b; Q_1, Q_2)\end{aligned} \tag{2.3}$$

Parton level cross sections are denoted with σ_{ik}, for hard process between partons i and k, and σ_{jl} for hard process between partons j and l. These are the same as for single parton scattering and are know for most of the processes of interest today. Quantity $\Gamma_{ij}(x_1, x_2, b; t_1, t_2)$ represents double parton distribution function which describes the probability of finding a parton i with momentum fraction x_1 at scale Q_1 inside a proton together with a parton j with momentum fraction x_2 at scale Q_2. Another parameter in this distribution function is b which describes transverse distance between two partons. Scales Q_1 and Q_2 and correspond to characteristic scales of hard processes A and B. For example in the framework of this thesis W boson production would correspond to process A and production of two b jets would correspond to process B. This study is described in detail in [19]. Usually, it is assumed that $\Gamma_{ij}(x_1, x_2, b; t_1, t_2)$ can be decomposed into two components, longitudinal and transversal in the following way:

$$\Gamma_{ij}(x_1, x_2, b; t_1, t_2) = D_h^{ij}(x_1, x_2; t_1, t_2) F_j^i(b) \tag{2.4}$$

The interpretation of the function $D_h^{ij}(x_1, x_2; t_1, t_2)$ within QCD is the probability of finding parton i with scale Q_1 and parton j with scale Q_2. These functions cannot be determined using perturbative QCD, thus good modeling and and correctly taking into account correlations between longitudinal momenta and transverse position is essential to making accurate cross section predictions.

More details on how to determine dPDFs can be found in [20], but in the simplest case $D_h^{ij}(x_1, x_2; t_1, t_2)$ can be taken as a product of single parton distribution fuctions taking into account effects like $x_1 + x_2 < 1$. Since $F_j^i(b)$ is the only part of $\sigma_{(A,B)}^{DPS}$ that depends only on b, integration over b can be performed giving an effective cross section $\sigma_e ff$ which is related to the size of the proton and can be seen as an effective area of the interaction. This approach yields a simplified expression for the double parton scattering cross section:

$$\sigma_{(A,B)}^{DPS} \sim \frac{1}{\sigma_e ff} \sigma_{(A)}^{SPS} \sigma_{(B)}^{SPS} \tag{2.5}$$

Here $\sigma_{(A)}^{SPS}$ and $\sigma_{(B)}^{SPS}$ are single parton scattering cross section which can be obtained using equation 2.2.

However, this factorized approach does not take into account some simple correlations like how finding a quark of some flavor affects the probability of finding another quark with the same flavor. While for some simple cases with low parton momentum fractions this factorized approach may give accurate results, for more complicated cases like calculating fiducial cross sections, acceptance cuts can spoil the equation. Thus, a simulation of the full kinematical effects is necessary.

First measurements of σ_{eff} have been performed by the AFS collaboration at the ISR which was $\sigma_{eff} \sim 5$ mb at 63GeV. Tevatron where both CDF and D0 collaborationsreported $\sigma_{eff} \sim 15$ mb which is roughly 20% of the total $p\bar{p}$ cross section at Tevatron energies. Their data also shows no sign of dependance on x in their measured σ_{eff} in the x ranges accessible. Later measurements performed by ATLAS ans CMS collaborations are in reasonable agreement with previous results. All results are summarized in Figure 2.11.

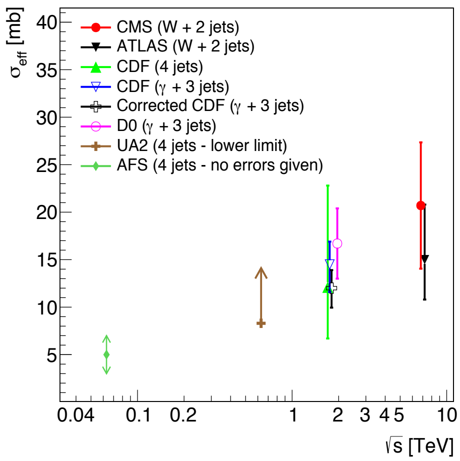

FIGURE 2.11: Center of mass energy dependence of σ_{eff} as reported from different collaborations. All these measurements use different approaches to estimate $\sigma_e ff$. [21]

Double parton scattering measurement at CMS is performed by selecting the events with a W + 2-jet final state where one hard interaction produces a W boson and another produces a dijet [22]. The W + 2-jet process is attractive because the muonic decay of the W provides a clean tag and the large dijet production cross section increases the probability of observing DPS. Events containing a W + 2-jet final state originating from single parton scattering (SPS) constitute an irreducible back- ground. Results were obtained by performing a template fit to two uncorrelated variables: the relative p_T ballance between two jets (Δp_T) and the angle between W boson and a dijet system. Obtained results again show that contribution of DPS to total cross section is $\sim$ 20% which is in good agreement with previous Tevatron results. The DPS contribution in the case od W + 2 b jets is estimated to be $\sim$ 15%. [23]

2.3 Previous measurements

Previous measurements of a W boson produced in association with b quarks have been performed on different experiments. However, the final states and phase space used in these measurements were different, which means that the results cannot be directly compared, but they can be compared with theoretical predictions. This process was measured for the first time at Tevatron with D0 and CDF experiments at $\sqrt{s} = 1.96$ TeV. The CDF collaboration published its result in 2009 and the cross-section measured is that of "jets from b-quarks produced with a W boson"[24]. The event selection is based on reconstructing a leptonically decaying W boson, and one or two jets where at least one has to be b-tagged. Events with jets from light quarks are vetoed with a cut on the secondary vertex mass. Contribution of other background events containing a b quark in final state (e.g. events with top quark) is estimated using Monte Carlo simulations. The measured cross section is 2.8 standard deviations higher than corresponding theoretical prediction. D0 collaboration published their result in 2012. with somewhat different phase space definition[25]. The difference with respect to the CDF measurement consists in the inclusion of the events with 3 jets and reduced pseudorapidity range in which the measurement was performed. The measurement technique is similar to that of CDF, although b-tagging algorithms were slightly different. The measured cross section was in good agreement with the Standard model prediction.

First measurements at the LHC were published by the ATLAS collaboration based on 36/pb of integrated luminosity at $\sqrt{s} = 7$ TeV. One year later they improved their measurement using 4.6/fb [26]. Selected events contain one reconstructed electron or muon, significant amount of missing transverse energy and one or two jets where exactly one is b-tagged. The phase space is divided in two regions, depending on the number of jets. Events with exactly 2 b jets and events with more than 2 jets are vetoed in order to suppress background events from top quark decay. The results are shown in Figure 2.12. The cross section measurement in the one jet region shows an excess corresponding to 1.5 standard deviations. In the two jet region, the measured cross section is in good agreement with theoretical predictions. A differential cross section measurement as a function of leading b jet transverse momentum has been performed for the first time and shown in figure 2.13. The cross section measurement in the one jet region is again higher that NLO predictions but within theoretical and experimental uncertainties. The cross section measured for the events with two jets is in good agreement with the theoretical prediction.

The CMS collaboration published its results corresponding to data collected during 2011.

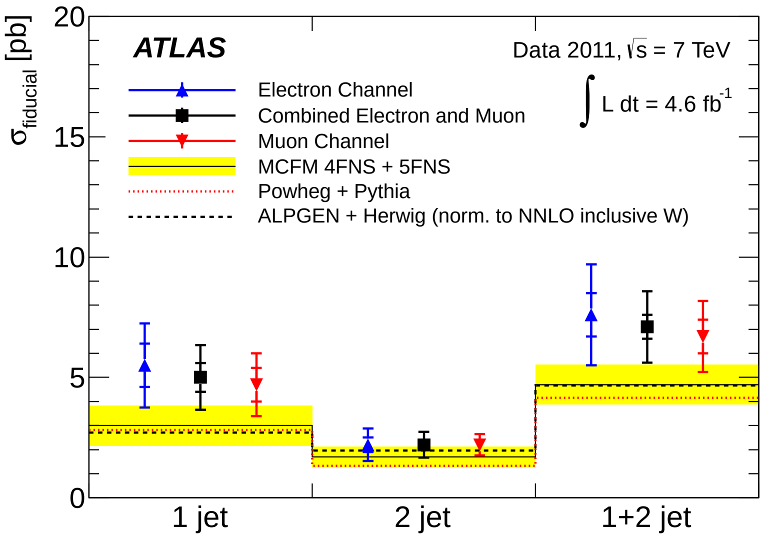

FIGURE 2.12: Measured fiducial cross-sections in the electron, muon, and combined electron and muon channels. The cross-sections are given in the 1-jet, 2-jet, and 1+2-jet fiducial regions.[26]

The measured events contained a muon and missing transverse energy in the final state, together with two b-tagged jets. The measured cross section is in excellent agreement with the Standard model prediction.[23]

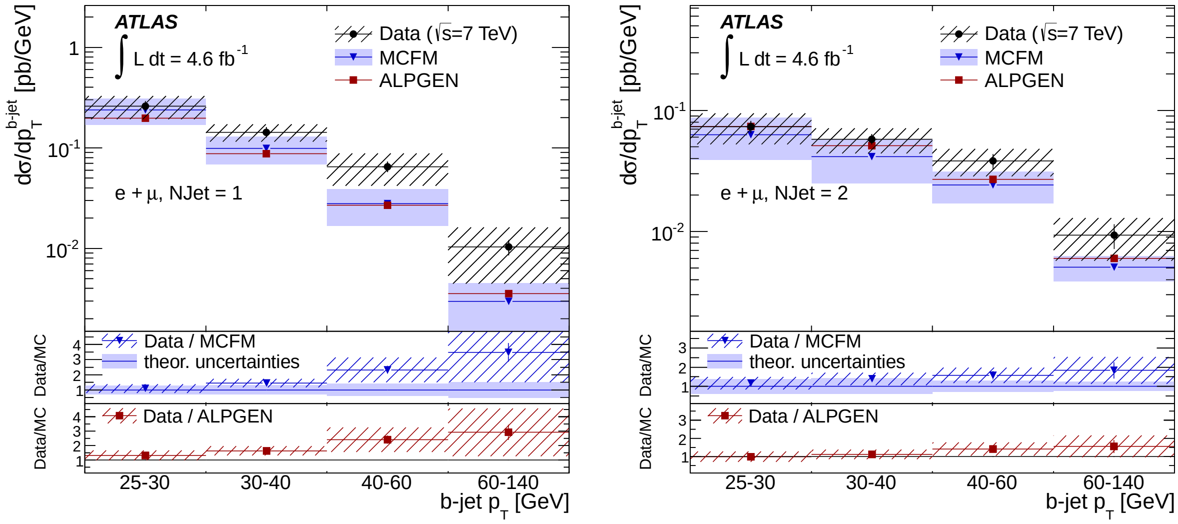

(A) (B)

FIGURE 2.13: Measured differential W+b-jets cross-sections as a function of leading b-jet p_T in the 1-jet (2.13a) and 2-jet (2.13b) fiducial regions, obtained by combining the muon and electron channel results. [26]

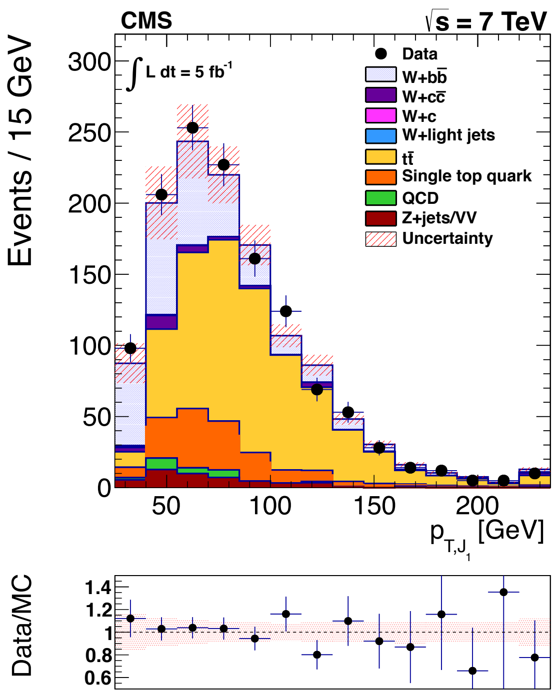

FIGURE 2.14: CMS Wbb total cross section measurement[23]

Chapter 3

Large Hadron Collider

Physics goals go here.

3.1 Design of the Large Hadron Collider

3.2 Performance

Since the start of the LHC in 2009, there were three years of machine operation, which yielded many physics results among which the discovery of Higgs boson reported by ATLAS and CMS collaborations. should be highlighted. First year of operation was devoted to commissioning and understanding machine characteristics with the emphasis on safety and testing machine protection systems. In 2011 new energy and instantaneous luminosity records were reached. These numbers were increased once again in 2012 with center of mass energy going to 8 TeV.

High bunch intensity with 50 ns bunch spacing was used in order to get a good instantaneous luminosity performance. This came at a cost of high number of collisions in one bunch crossing (pile-up) which was in 2012 around 12 collisions, and in some cases this

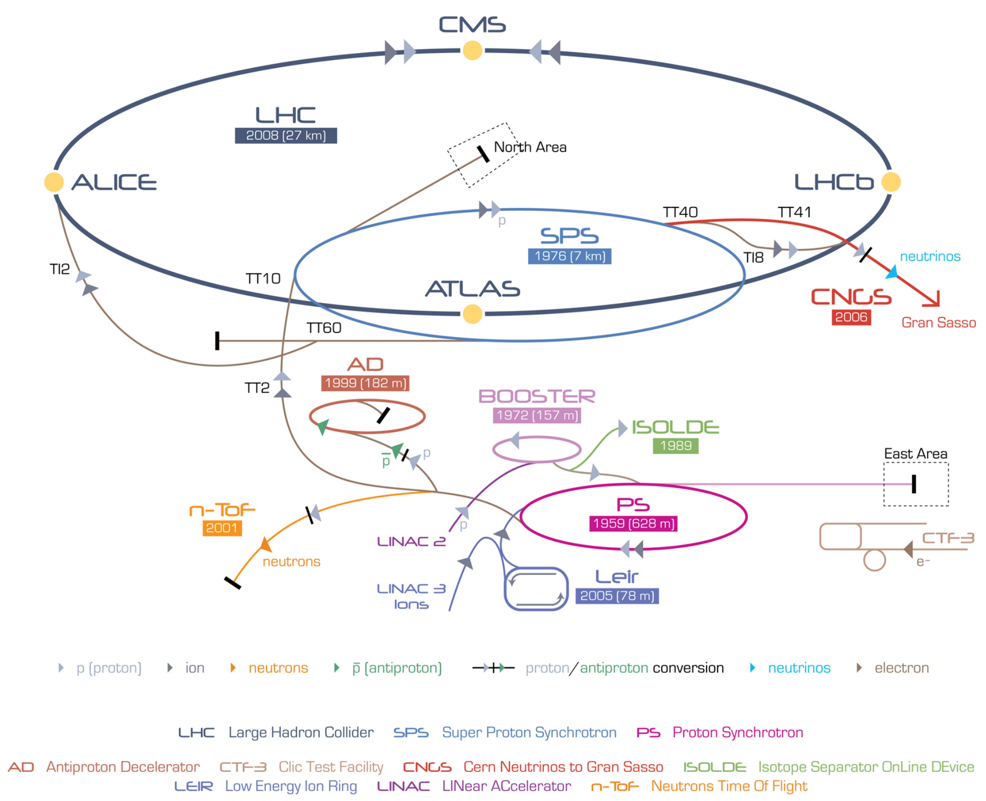

FIGURE 3.1: Schematics of Large Hadron Collider

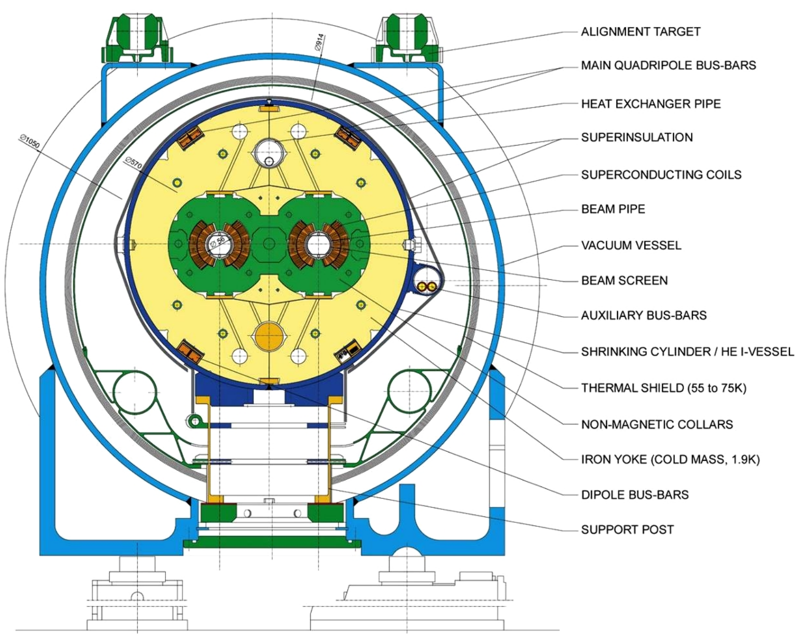

FIGURE 3.2: Schematics of Dipole magnets

number went as high as 20 interactions. With the increase of instantaneous luminosity in 2012, number of pile-up interactions was on the average around 30. Besides proton-proton collisions, LHC successfully delivered lead-lead ion runs in 2010 and 2011. primarily for the ALICE experiment, but also for CMS and ATLAS. At the start of 2013. there was also a successful proton-lead run performed for the first time.

Table 3.1: LHC performance in 2012

Parameter	Design value	Value in 2012
Beam energy [TeV]	7	4
Bunch spacing [ns]	25	50
Number of bunches	2808	1374
Protons per bunch	1.15×10^{11}	$1.6\text{-}1.7\times10^{11}$
Peak luminosity [$cm^{-2}s^{-1}$]	1×10^{34}	7.7×10^{33}
Max. number of events per bunch crossing	19	≈ 40
Stored beam energy [MJ]	362	≈ 140

LHC head achieved very good luminosity performance during pat years mainly because of the excellent beam quality delivered by the injectors with significantly more protons than nominal and with lower emittances. Since the LHC was capable to absorb these beams, it was chosen to continue to operate with 50 ns bunch spacing. This meant higher pile-up which had to be dealt with by the experiments.

Table 3.2: LHC performance highlights

Max. luminosity delivered in one fill	237 pb^{-1}
Max. luminosity delivered in 7 days	1.35 fb^{-1}
Longest time in stable beams (2012)	22.8 hours
Longest time in stable beams over 7 days	91.8 hours (55%)

Following a two year shutdown, LHC is anticipating operations at even higher energies of 6.5 TeV and later 7 TeV. The long term plan includes even higher peak luminosities, installation of the new injector complex and later the beginning of HL-LHC era. The timeline will, of course, be highly affected by the performance and results of the next run.

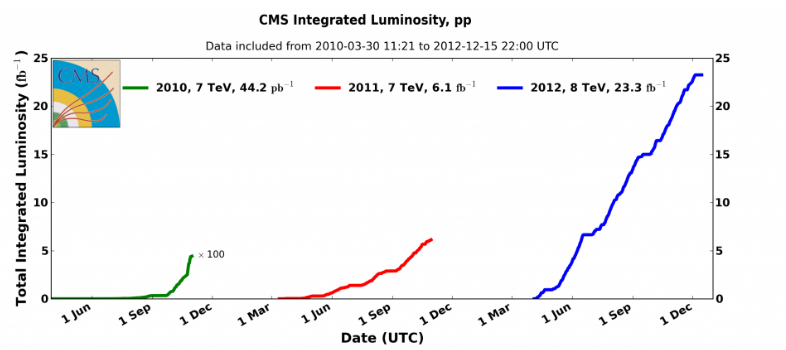

FIGURE 3.3: Luminosity delivered to the CMS experiment

Chapter 4

Compact Muon Solenoid

4.1 Inner tracker system

Lorem ipsum dolor sit amet, consectetur adipiscing elit. Aliquam ultricies lacinia euismod. Nam tempus risus in dolor rhoncus in interdum enim tincidunt. Donec vel nunc neque. In condimentum ullamcorper quam non consequat. Fusce sagittis tempor feugiat. Fusce magna erat, molestie eu convallis ut, tempus sed arcu. Quisque molestie, ante a tincidunt ullamcorper, sapien enim dignissim lacus, in semper nibh erat lobortis purus. Integer dapibus ligula ac risus convallis pellentesque.

4.1.1 Pixel Detector

Nunc posuere quam at lectus tristique eu ultrices augue venenatis. Vestibulum ante ipsum primis in faucibus orci luctus et ultrices posuere cubilia Curae; Aliquam erat volutpat. Vivamus sodales tortor eget quam adipiscing in vulputate ante ullamcorper. Sed eros ante, lacinia et sollicitudin et, aliquam sit amet augue. In hac habitasse platea dictumst.

4.1.1.1 Lorentz angle measurement

4.1.2 Strip detector

Morbi rutrum odio eget arcu adipiscing sodales. Aenean et purus a est pulvinar pellentesque. Cras in elit neque, quis varius elit. Phasellus fringilla, nibh eu tempus venenatis, dolor elit posuere quam, quis adipiscing urna leo nec orci. Sed nec nulla auctor odio aliquet consequat. Ut nec nulla in ante ullamcorper aliquam at sed dolor. Phasellus fermentum magna in augue gravida cursus. Cras sed pretium lorem. Pellentesque eget ornare odio. Proin accumsan, massa viverra cursus pharetra, ipsum nisi lobortis velit, a malesuada dolor lorem eu neque.

4.2 Electromagnetic calorimeter

Sed ullamcorper quam eu nisl interdum at interdum enim egestas. Aliquam placerat justo sed lectus lobortis ut porta nisl porttitor. Vestibulum mi dolor, lacinia molestie gravida at, tempus vitae ligula. Donec eget quam sapien, in viverra eros. Donec pellentesque justo a massa fringilla non vestibulum metus vestibulum. Vestibulum in orci quis felis tempor lacinia. Vivamus ornare ultrices facilisis. Ut hendrerit volutpat vulputate. Morbi condimentum venenatis augue, id porta ipsum vulputate in. Curabitur luctus tempus justo. Vestibulum risus lectus, adipiscing nec condimentum quis, condimentum nec nisl. Aliquam dictum sagittis velit sed iaculis. Morbi tristique augue sit amet nulla pulvinar id facilisis ligula mollis. Nam elit libero, tincidunt ut aliquam at, molestie in quam. Aenean rhoncus vehicula hendrerit.

4.3 Hadronic calorimeter

4.4 Solenoid

4.5 Muon chambers

4.6 Trigger

4.7 Data acquisition system

Chapter 5

Physics objects definitions

5.1 Electrons

Lorem ipsum dolor sit amet, consectetur adipiscing elit. Aliquam ultricies lacinia euismod. Nam tempus risus in dolor rhoncus in interdum enim tincidunt. Donec vel nunc neque. In condimentum ullamcorper quam non consequat. Fusce sagittis tempor feugiat. Fusce magna erat, molestie eu convallis ut, tempus sed arcu. Quisque molestie, ante a tincidunt ullamcorper, sapien enim dignissim lacus, in semper nibh erat lobortis purus. Integer dapibus ligula ac risus convallis pellentesque.

5.1.1 Electron identification

Nunc posuere quam at lectus tristique eu ultrices augue venenatis. Vestibulum ante ipsum primis in faucibus orci luctus et ultrices posuere cubilia Curae; Aliquam erat volutpat. Vivamus sodales tortor eget quam adipiscing in vulputate ante ullamcorper. Sed eros ante, lacinia et sollicitudin et, aliquam sit amet augue. In hac habitasse platea dictumst.

5.1.2 Electron isolation

Morbi rutrum odio eget arcu adipiscing sodales. Aenean et purus a est pulvinar pellentesque. Cras in elit neque, quis varius elit. Phasellus fringilla, nibh eu tempus venenatis, dolor elit posuere quam, quis adipiscing urna leo nec orci. Sed nec nulla auctor odio aliquet consequat. Ut nec nulla in ante ullamcorper aliquam at sed dolor. Phasellus fermentum magna in augue gravida cursus. Cras sed pretium lorem. Pellentesque eget ornare odio. Proin accumsan, massa viverra cursus pharetra, ipsum nisi lobortis velit, a malesuada dolor lorem eu neque.

5.2 Muons

Sed ullamcorper quam eu nisl interdum at interdum enim egestas. Aliquam placerat justo sed lectus lobortis ut porta nisl porttitor. Vestibulum mi dolor, lacinia molestie gravida at, tempus vitae ligula. Donec eget quam sapien, in viverra eros. Donec pellentesque justo a massa fringilla non vestibulum metus vestibulum. Vestibulum in orci quis felis tempor lacinia. Vivamus ornare ultrices facilisis. Ut hendrerit volutpat vulputate. Morbi condimentum venenatis augue, id porta ipsum vulputate in. Curabitur luctus tempus justo. Vestibulum risus lectus, adipiscing nec condimentum quis, condimentum nec nisl. Aliquam dictum sagittis velit sed iaculis. Morbi tristique augue sit amet nulla pulvinar id facilisis ligula mollis. Nam elit libero, tincidunt ut aliquam at, molestie in quam. Aenean rhoncus vehicula hendrerit.

5.2.1 Muon identification

5.2.2 Muon isolation

5.3 Jets

5.3.1 Jet identification

5.3.2 Jets from b quarks

5.4 Missing transverse energy

5.5 W boson candidates

Chapter 6

Signal selection

6.1 Analysis strategy

Lorem ipsum dolor sit amet, consectetur adipiscing elit. Aliquam ultricies lacinia euismod. Nam tempus risus in dolor rhoncus in interdum enim tincidunt. Donec vel nunc neque. In condimentum ullamcorper quam non consequat. Fusce sagittis tempor feugiat. Fusce magna erat, molestie eu convallis ut, tempus sed arcu. Quisque molestie, ante a tincidunt ullamcorper, sapien enim dignissim lacus, in semper nibh erat lobortis purus. Integer dapibus ligula ac risus convallis pellentesque.

6.1.1 Subsection 1

Nunc posuere quam at lectus tristique eu ultrices augue venenatis. Vestibulum ante ipsum primis in faucibus orci luctus et ultrices posuere cubilia Curae; Aliquam erat volutpat. Vivamus sodales tortor eget quam adipiscing in vulputate ante ullamcorper. Sed eros ante, lacinia et sollicitudin et, aliquam sit amet augue. In hac habitasse platea dictumst.

6.1.2 Subsection 2

Morbi rutrum odio eget arcu adipiscing sodales. Aenean et purus a est pulvinar pellentesque. Cras in elit neque, quis varius elit. Phasellus fringilla, nibh eu tempus venenatis, dolor elit posuere quam, quis adipiscing urna leo nec orci. Sed nec nulla auctor odio aliquet consequat. Ut nec nulla in ante ullamcorper aliquam at sed dolor. Phasellus fermentum magna in augue gravida cursus. Cras sed pretium lorem. Pellentesque eget ornare odio. Proin accumsan, massa viverra cursus pharetra, ipsum nisi lobortis velit, a malesuada dolor lorem eu neque.

6.2 Background estimation

Sed ullamcorper quam eu nisl interdum at interdum enim egestas. Aliquam placerat justo sed lectus lobortis ut porta nisl porttitor. Vestibulum mi dolor, lacinia molestie gravida at, tempus vitae ligula. Donec eget quam sapien, in viverra eros. Donec pellentesque justo a massa fringilla non vestibulum metus vestibulum. Vestibulum in orci quis felis tempor lacinia. Vivamus ornare ultrices facilisis. Ut hendrerit volutpat vulputate. Morbi condimentum venenatis augue, id porta ipsum vulputate in. Curabitur luctus tempus justo. Vestibulum risus lectus, adipiscing nec condimentum quis, condimentum nec nisl. Aliquam dictum sagittis velit sed iaculis. Morbi tristique augue sit amet nulla pulvinar id facilisis ligula mollis. Nam elit libero, tincidunt ut aliquam at, molestie in quam. Aenean rhoncus vehicula hendrerit.

Chapter 7

Prosireni sazetak:

7.1 Main Section 1

Lorem ipsum dolor sit amet, consectetur adipiscing elit. Aliquam ultricies lacinia euismod. Nam tempus risus in dolor rhoncus in interdum enim tincidunt. Donec vel nunc neque. In condimentum ullamcorper quam non consequat. Fusce sagittis tempor feugiat. Fusce magna erat, molestie eu convallis ut, tempus sed arcu. Quisque molestie, ante a tincidunt ullamcorper, sapien enim dignissim lacus, in semper nibh erat lobortis purus. Integer dapibus ligula ac risus convallis pellentesque.

7.1.1 Subsection 1

Nunc posuere quam at lectus tristique eu ultrices augue venenatis. Vestibulum ante ipsum primis in faucibus orci luctus et ultrices posuere cubilia Curae; Aliquam erat volutpat. Vivamus sodales tortor eget quam adipiscing in vulputate ante ullamcorper. Sed eros ante, lacinia et sollicitudin et, aliquam sit amet augue. In hac habitasse platea dictumst.

7.1.2 Subsection 2

Morbi rutrum odio eget arcu adipiscing sodales. Aenean et purus a est pulvinar pellentesque. Cras in elit neque, quis varius elit. Phasellus fringilla, nibh eu tempus venenatis, dolor elit posuere quam, quis adipiscing urna leo nec orci. Sed nec nulla auctor odio aliquet consequat. Ut nec nulla in ante ullamcorper aliquam at sed dolor. Phasellus fermentum magna in augue gravida cursus. Cras sed pretium lorem. Pellentesque eget ornare odio. Proin accumsan, massa viverra cursus pharetra, ipsum nisi lobortis velit, a malesuada dolor lorem eu neque.

7.2 Main Section 2

Sed ullamcorper quam eu nisl interdum at interdum enim egestas. Aliquam placerat justo sed lectus lobortis ut porta nisl porttitor. Vestibulum mi dolor, lacinia molestie gravida at, tempus vitae ligula. Donec eget quam sapien, in viverra eros. Donec pellentesque justo a massa fringilla non vestibulum metus vestibulum. Vestibulum in orci quis felis tempor lacinia. Vivamus ornare ultrices facilisis. Ut hendrerit volutpat vulputate. Morbi condimentum venenatis augue, id porta ipsum vulputate in. Curabitur luctus tempus justo. Vestibulum risus lectus, adipiscing nec condimentum quis, condimentum nec nisl. Aliquam dictum sagittis velit sed iaculis. Morbi tristique augue sit amet nulla pulvinar id facilisis ligula mollis. Nam elit libero, tincidunt ut aliquam at, molestie in quam. Aenean rhoncus vehicula hendrerit.

Appendix A

Lorentz angle measurement in Pixel detector

Lorentz angle is measured by using grazing angle method described in detail in [27]. From the individual signals in the detector, using reconstruction algorithms, tracks of muon candidates are obtained. From these reconstructed track it is possible to extract the entry point (x_{reco},y_{reco}) to each layer of the detector. Distance between reconstructed entry point and the actual hit in the detector is then defined as (Δx,Δy):

$$\Delta x = x_{center} - x_{reco} \tag{A.1}$$

$$\Delta y = y_{center} - y_{reco} \tag{A.2}$$

where (x_{center},y_{center}) is the position of each individual pixel center in the observed cluster. Drift of the electrons can be determined using three impact angles defined in the following way:

$$\tan\alpha = \frac{p_z}{p_x} \tag{A.3}$$

$$\tan\beta = \frac{p_z}{p_y} \tag{A.4}$$

$$\tan\gamma = \frac{p_x}{p_y} \tag{A.5}$$

where p_x,p_y and p_z are momentum components in local coordinate system which are calculated from reconstructed track parameters (Fig. A.1).

Drift of the electrons depends on the depth at which electrons are created. Depth of the

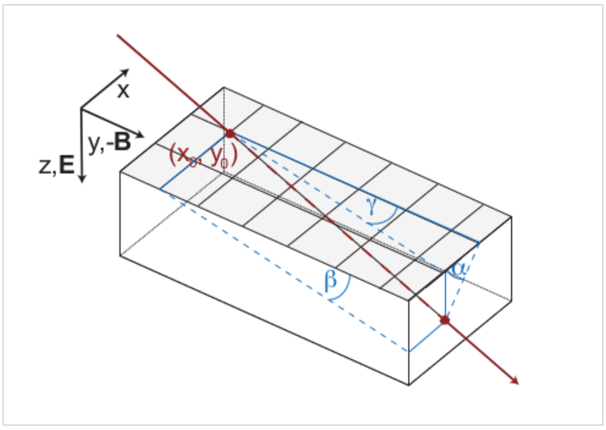

FIGURE A.1: Angle definitions for grazing angle method.

electron production z and drift due to magnetic field d are defined:

$$z = \Delta y \tan\beta \tag{A.6}$$

$$d = \Delta x - \Delta y \tan\gamma \tag{A.7}$$

This procedure is repeated for each pixel over many tracks in order to obtain charge drift distance vs depth. The Lorentz angle is the slope of this distribution. Without a magnetic field, the direction of the clusters largest extension is parallel to the track projection on the (x, y) plane. The average drift distance of an electron created at a certain depth is obtained from Fig. A.2. A linear fit is performed over the total depth of the detector excluding the first and last 50 μ where the charge drift is systematically displaced by the finite size of the pixel cell (Fig:A.3).

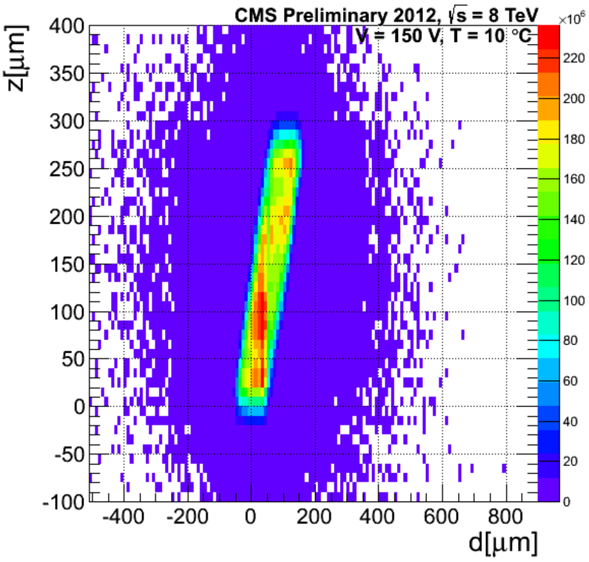

FIGURE A.2: Depth at which electrons in silicon bulk were produced as a function of Lorentz drift.

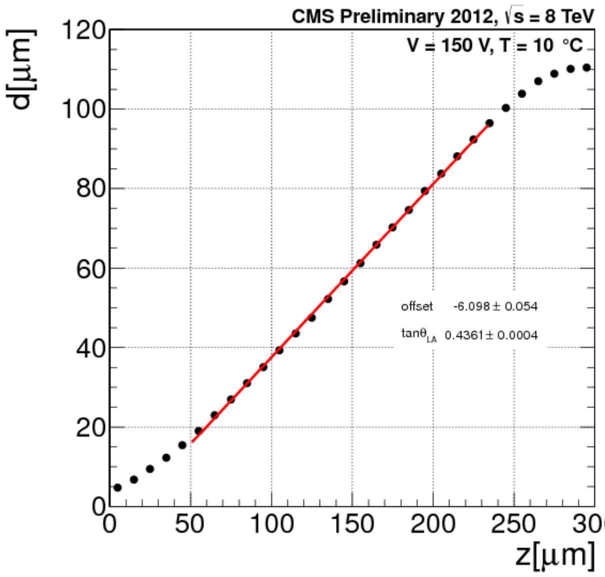

FIGURE A.3: The average drift of electrons as a function of the production depth. Slope of the linear fit result is the $tan\theta_L$.

In order to obtain a good measurement, it is important to use clean tracks. Therefore, it required to have a well reconstructed muon tracks with $p_T > 3$GeV and $\chi^2/ndof < 2$ which are required to have shallow impact angle with respect to local y direction with cluster size of at least 4 pixels in this direction. Summary of the selection criteria can be found in table A.1.

TABLE A.1: Selection criteria for Lorentz angle measurement

Cluster size in y	> 3
Track p_t	> 3GeV/c
χ^2/ndof	< 2
Hit residuals	$< 50\mu m$
Cluster charge	< 120000e

Figure A.4 shows how Lorentz angle changes with integrated luminosity. Results are shown for 23fb^{-1} of delivered luminosity in 2012. Increase in Lorentz angle measured with grazing angle method has been observed in all layers, with largest effect (6%) visible in layer 1 over this period of data taking.

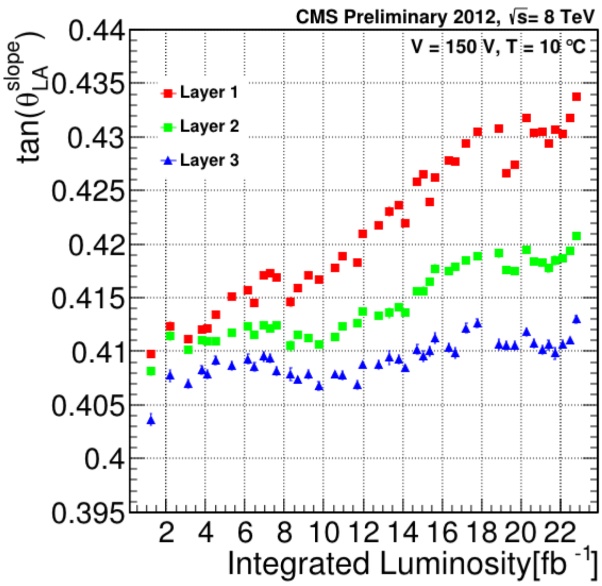

FIGURE A.4: Lorentz angle as a function of integrated luminosity for 2012.

Bibliography

[1] Georges Aad et al. Observation of a new particle in the search for the Standard Model Higgs boson with the ATLAS detector at the LHC. *Phys.Lett.*, B716:1–29, 2012.

[2] Serguei Chatrchyan et al. Observation of a new boson at a mass of 125 GeV with the CMS experiment at the LHC. *Phys.Lett.*, B716:30–61, 2012.

[3] D. Griffiths. *Introduction to Elementary Particles*. John Wiley & Sons, New York, USA, 1987.

[4] Makoto Kobayashi and Toshihide Maskawa. CP Violation in the Renormalizable Theory of Weak Interaction. *Prog.Theor.Phys.*, 49:652–657, 1973.

[5] S. W. Herb, D. C. Hom, L. M. Lederman, J. C. Sens, H. D. Snyder, J. K. Yoh, J. A. Appel, B. C. Brown, C. N. Brown, W. R. Innes, K. Ueno, T. Yamanouchi, A. S. Ito, H. Jöstlein, D. M. Kaplan, and R. D. Kephart. Observation of a dimuon resonance at 9.5 gev in 400-gev proton-nucleus collisions. *Phys. Rev. Lett.*, 39:252–255, Aug 1977.

[6] G. Arnison et al. Experimental Observation of Isolated Large Transverse Energy Electrons with Associated Missing Energy at s**(1/2) = 540-GeV. *Phys.Lett.*, B122:103–116, 1983.

[7] M. Banner et al. Observation of Single Isolated Electrons of High Transverse Momentum in Events with Missing Transverse Energy at the CERN anti-p p Collider. *Phys.Lett.*, B122:476–485, 1983.

[8] John M. Campbell. Overview of the theory of W/Z + jets and heavy flavor. 2008.

[9] Michelangelo L. Mangano. Production of W plus heavy quark pairs in hadronic collisions. *Nucl.Phys.*, B405:536–554, 1993.

[10] Serguei Chatrchyan et al. Search for the standard model Higgs boson produced in association with a W or a Z boson and decaying to bottom quarks. *Phys.Rev.*, D89(1):012003, 2014.

[11] Serguei Chatrchyan et al. Evidence for the direct decay of the 125 GeV Higgs boson to fermions. *Nature Phys.*, 10:557–560, 2014.

[12] K.A. Olive et al. Review of Particle Physics. *Chin.Phys.*, C38:090001, 2014.

[13] John M. Campbell, J.W. Huston, and W.J. Stirling. Hard Interactions of Quarks and Gluons: A Primer for LHC Physics. *Rept.Prog.Phys.*, 70:89, 2007.

[14] A.D. Martin, W.J. Stirling, R.S. Thorne, and G. Watt. Parton distributions for the LHC. *Eur.Phys.J.*, C63:189–285, 2009.

[15] Fabio Maltoni, Giovanni Ridolfi, and Maria Ubiali. b-initiated processes at the LHC: a reappraisal. *JHEP*, 1207:022, 2012.

[16] R. Keith Ellis and Sinisa Veseli. Strong radiative corrections to W b anti-b production in p anti-p collisions. *Phys.Rev.*, D60:011501, 1999.

[17] Michelangelo L. Mangano, Mauro Moretti, and Roberto Pittau. Multijet matrix elements and shower evolution in hadronic collisions: $Wb\bar{b} + n$ jets as a case study. *Nucl.Phys.*, B632:343–362, 2002.

[18] F. Febres Cordero, L. Reina, and D. Wackeroth. NLO QCD corrections to W boson production with a massive b-quark jet pair at the Tevatron p anti-p collider. *Phys.Rev.*, D74:034007, 2006.

[19] Seth Quackenbush, Edmond L. Berger, C.B. Jackson, and Gabe Shaughnessy. LHC Sensitivity to $Wb\bar{b}$ Production via Double Parton Scattering. 2011.

[20] Jonathan R. Gaunt and W. James Stirling. Double Parton Distributions Incorporating Perturbative QCD Evolution and Momentum and Quark Number Sum Rules. *JHEP*, 1003:005, 2010.

[21] Sunil Bansal, Paolo Bartalini, Boris Blok, Diego Ciangottini, Markus Diehl, et al. Progress in Double Parton Scattering Studies. 2014.

[22] Serguei Chatrchyan et al. Study of double parton scattering using W + 2-jet events in proton-proton collisions at $\sqrt{s} = 7$ TeV. *JHEP*, 1403:032, 2014.

[23] Serguei Chatrchyan et al. Measurement of the production cross section for a W boson and two b jets in pp collisions at $\sqrt{s}$=7 TeV. *Phys.Lett.*, B735:204–225, 2014.

[24] T. Aaltonen et al. First Measurement of the b-jet Cross Section in Events with a W Boson in p anti-p Collisions at s**(1/2) = 1.96-TeV. *Phys.Rev.Lett.*, 104:131801, 2010.

[25] V.M. Abazov et al. Measurement of the $p\bar{p} \to W + b + X$ production cross section at $\sqrt{s} = 1.96$ TeV. *Phys.Lett.*, B718:1314–1320, 2013.

[26] Georges Aad et al. Measurement of the cross-section for W boson production in association with b-jets in pp collisions at $\sqrt{s} = 7$ TeV with the ATLAS detector. *JHEP*, 1306:084, 2013.

[27] B Henrich and R Kaufmann. Lorentz-angle in irradiated silicon. *Nucl. Instrum. Methods Phys. Res., A*, 477(1-3):304–307, 2002.